

A Graph-based Method to Extract Broken Rotor Bar Fault Signature in Varying Speed Operation

Zhang, Zhe; Liu, Dehong

TR2021-135 November 13, 2021

Abstract

In this paper, a graph-based filtering technique is proposed to identify fault signature of broken rotor bar in inverter-fed induction motor under varying-speed operation. Simulation results verified the effectiveness of the proposed method.

International Conference on Electrical Machines and Systems (ICEMS) 2021

A Graph-based Method to Extract Broken-Rotor-Bar Fault Signature in Varying Speed Operation

Zhe Zhang^{1,2} and Dehong Liu^{1,*}

¹ *Mitsubishi Electric Research Laboratories (MERL), Cambridge, MA, USA*

² *University of Connecticut, USA*

Email: zhe.4.zhang@uconn.edu, liudh@merl.com

Abstract—Motor current signature analysis (MCSA) has been a mature technique for fault detection in line-fed induction motors for decades. Since nowadays most induction motors are driven by inverters, it is challenging to detect faults in inverter-fed induction motors due to the operation of varying speed and varying load. In this paper, we study broken-bar fault detection in inverter-fed induction motors under varying speed conditions. By representing the stator current using a complex space vector, we define a new fault signature of continuous varying frequency. To effectively extract the newly defined broken-bar fault signature, we propose a graph-based method in which we solve an optimization problem of graph model with constraints imposing smoothness and sparsity of the spectrum. Simulation results demonstrate the effectiveness of the proposed method.

Index Terms—Induction machine, Broken rotor bar, Fault signature, Complex space vector, Graph model.

NOMENCLATURE

r_s	Stator resistance,
r_r	Rotor resistance,
L_s	Stator inductance,
L_r	Rotor inductance,
L_m	Mutual inductance,
λ_s	Stator flux linkage,
λ_r	Rotor flux linkage,
p	Differential operation,
J	Moment of inertia,
T_e	Electromagnetic torque,
T_L	Load torque.

I. INTRODUCTION

Three-phase induction motors (IMs) have been the major workforce in the industry due to their excellent performance, high robustness, and simplicity of construction [1]. However, IMs are subjected to different types of faults, including broken rotor bar fault. Once a broken bar fault occurs, excessive vibration, poor starting performance, and torque fluctuation will be induced during operation. Even worse, it may cause catastrophic failure of the whole motor drive system. Therefore, it is of great importance to monitor machine condition and to detect motor faults in motor drive systems.

The cause-effect chain for rotor faults has been well investigated and demonstrated in [2]. In healthy conditions, three-phase stator winding impedances are identical and induced rotor-bar currents are well balanced. Frequency components at f and sf exist in the stator current and the rotor current, respectively, where f is the supply frequency and s is the slip. Once a rotor bar is broken, the corresponding circuit branch is open. A reverse rotating magnetic field is produced due to the loss of rotor circuit's symmetry and a negative frequency component at $(-sf)$ appears in the rotor currents. Such negative frequency component produces the first fault frequency component at $(1-2s)f$ in the stator current, causing a pulsating torque and a speed oscillation at the frequency of $2sf$. Consequently, a set of new frequency components at frequencies of $(1\pm 2k)sf$, where $k = 0, 1, 2, \dots$, appear in the spectrum of stator currents as well as a new set of frequency components at frequencies of $\pm(1+2k)sf$ in rotor currents [3]. In general, broken-bar fault diagnostic techniques are focused on detecting the fault dominant component at frequency of $(1-2s)f$ in the stator current.

Motor current signature analysis (MCSA) has been widely used in IM fault detection for decades because of its effectiveness and noninvasive property. Based on the stator current frequency spectrum, MCSA methods aim to extract characteristic frequency components for different types of faults [4]. However, the most common practice of MCSA in rotor fault detection is dealing with line-fed IMs under stationary conditions. Since nowadays voltage source inverters (VSI) driven IMs are becoming popular in industrial environments for the sake of efficiency and carbon neutrality, where stationary operations are quite unusual, conventional fast Fourier transform (FFT) based MCSA methods are either no longer applicable or with poor detection performance.

In recent years, researchers have developed rotor fault detection methods under non-stationary conditions. For example, CusidÓCusido *et al.* [5] proposed the short-time Fourier transform (STFT) in combination with a Wavelet analysis to detect rotor fault with improved results. In [6], an adaptive transform utilizes a function called the time-frequency atom that allows for precise observation of fault components in transient regimes. An application of multi-rate digital signal processing for rotor fault detection can be found in [7].

This work was finished when Zhe Zhang was an intern at MERL.

These methods allow tracking the fault-related frequency by performing relevant time-frequency (t-f) transform. The drawback is that the energy of the fault-related frequency component is much lower than the fundamental one, which makes it difficult to differentiate due to spectral leakage [8]. To improve the frequency spectrum resolution, Liu [9] proposed an off-the-grid compressive sensing method to achieve a super spectral resolution such that the fault characteristic frequency component can be well resolved even with a short-time current measurement, assuming the motor speed and the load are constant in the short measurement period. However, the compressive sensing based spectrum analysis method may suffer from noisy measurements. Some researchers have proposed the use of demodulation techniques aiming to eliminate the fundamental supply frequency and extract a reliable fault indicator based on stator current measurement [8], [10], [11]. The demodulation process essentially shifts the stator current spectrum along the frequency domain so that the fundamental component becomes DC (zero frequency). The masking effect of spectral leakage then can be largely eliminated by filtering the DC component in the demodulated signal. However, the noise issue is still not well addressed in these methods.

In this paper, we study the broken-bar fault signature under varying speed and varying load conditions. A new fault signature pattern can be observed by applying complex vector transformation to the stator currents. Such manipulation similarly transforms the overwhelming fundamental component to DC value and makes it easier to identify the fault-related component in the stator current spectrum. In order to effectively extract broken-bar fault signature of induction motors under varying operation conditions, we model the fault signature as a graph signal with a continuously changing and sparse frequency component. Following the idea of graph model, we propose a graph-based method to extract the fault signature by solving an optimization problem with constraints imposing sparsity and smoothness of the fault signature in the stator current spectrogram computed using STFT.

The rest of this paper is organized as follows. The dynamic model of induction machine under the complex space vector framework is introduced in Section II. In Section III, a graph-based method is proposed to effectively extract the fault signature. Simulation results are presented in Section IV to demonstrate the effectiveness of our proposed method. Section V concludes the paper.

II. COMPLEX VECTOR MODEL OF INDUCTION MACHINE WITH BROKEN ROTOR BARS

In this section, a detailed mathematical derivation of the induction machine with broken rotor bars will be discussed based on the complex space-vector notation and coupled magnetic circuit theory.

A. Complex Space Vectors for Stator/Rotor State variables

We consider a three phase squirrel-cage induction motor with n rotor bars (phases) on the rotor side. An equivalent circuit model of the squirrel-cage induction motor is shown in

Fig. 1. Each rotor bar is represented by an equivalent resistance R_b and an equivalent inductance L_b , and each segment of end ring is presented by a resistance R_e and an inductance L_e . This model is based on magnetic circuit theory considering the actual non-sinusoidal rotor bar distribution [12].

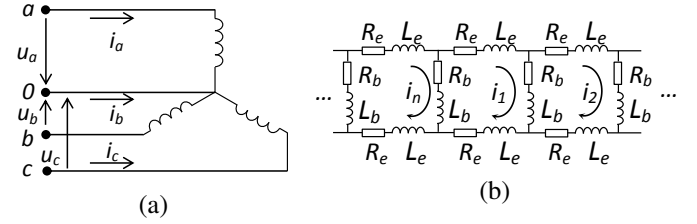


Fig. 1. Equivalent circuit of (a) stator windings and (b) rotor bars in the squirrel-cage induction motor

For any three phase variable $\{x_a, x_b, x_c\}$, which can be voltage, current, or flux, etc., we define a corresponding complex state variable \underline{X}_s on the stator side as

$$\underline{X}_s = \frac{2}{3} \begin{bmatrix} 1 & \underline{a} & \underline{a}^2 \end{bmatrix} \begin{bmatrix} x_a \\ x_b \\ x_c \end{bmatrix} = \frac{2}{3} (x_a + \underline{a}x_b + \underline{a}^2x_c), \quad (1)$$

where $\underline{a} = e^{j(2\pi/3)}$.

Similarly, for any rotor variable $\{y_1, y_2, \dots, y_n\}$, we define a corresponding complex state variable \underline{Y}_r on the rotor side as

$$\underline{Y}_r = \frac{2}{n} \begin{bmatrix} 1 & \underline{b} & \dots & \underline{b}^{n-1} \end{bmatrix} \begin{bmatrix} y_1 \\ y_2 \\ \vdots \\ y_n \end{bmatrix} = \frac{2}{n} (y_1 + \underline{b}y_2 + \dots + \underline{b}^{n-1}y_n), \quad (2)$$

where $\underline{b} = e^{j(2\pi/n)}$.

B. Modeling the Effect of Broken Rotor Bars

The electrical behavior of an induction machine in complex space-vector notation for stator and rotor can be summarized respectively as [13]

$$\begin{aligned} \underline{V}_s &= r_s \dot{\underline{i}}_s + p \underline{\lambda}_s \\ &= r_s \dot{\underline{i}}_s + L_s p \dot{\underline{i}}_s + \frac{n}{2} L_m e^{j(\theta_r + \frac{\alpha_r}{2})} (p + j\omega_r) \dot{\underline{i}}_r, \end{aligned} \quad (3)$$

and

$$\begin{aligned} \underline{0}_r &= r_r \dot{\underline{i}}_r + p \underline{\lambda}_r \\ &= r_r \dot{\underline{i}}_r + L_r p \dot{\underline{i}}_r + \frac{3}{2} L_m e^{j(\theta_r + \frac{\alpha_r}{2})} (p - j\omega_r) \dot{\underline{i}}_s, \end{aligned} \quad (4)$$

where θ_r is the rotor angle; $\omega_r = p\theta_r$ is the rotor angular frequency; α_r is the angle between two adjacent rotor bars; $\underline{0}_r$ represents the zero voltage vector due to the squirrel cage; and r_r is the equivalent rotor resistance in the subspace defined by the space-vector transformation which can be expressed as $r_r = 2R_e + 2R_b(1 - \cos \alpha_r)$.

The mechanical behavior of an induction machine can be summarized as

$$T_e = i_s^T \frac{\partial L_{sr}}{\partial \theta_r} i_r = -\left(\frac{3}{2}\right)\left(\frac{n}{2}\right)L_m \text{Im}\{e^{j(\theta_r + \frac{\alpha_r}{2})} \underline{i}_s^* \underline{i}_r\}, \quad (5)$$

$$T_e - T_l = J \frac{d\omega_r}{dt}. \quad (6)$$

Assuming the i -th rotor bar begins to degrade, one can define an increased rotor resistance R_b so that the induced rotor bar voltage in complex space-vector notation can be expressed as

$$\underline{v}_{brb_i} = \frac{2}{n} b^{i-1} v_{brb_i}. \quad (7)$$

To account for any degraded rotor bars into the induced rotor voltage, the following equation holds

$$\underline{v}_{brb_r} = \sum_i \underline{v}_{brb_i}. \quad (8)$$

Note that there are sinusoidal couplings between the stator and rotor circuits which can be eliminated by referring all the equations to a common reference frame. Apply the vector transformation referenced to stationary frame

$$\underline{X}_{qds} = \frac{2}{3} e^{-j\theta} \underline{X}_s, \quad (9)$$

$$\underline{Y}_{qdr} = \frac{2}{3} \sqrt{\frac{n}{3}} e^{j(\theta_r + \frac{\alpha_r}{2} - \theta)} \underline{Y}_r. \quad (10)$$

The equations for voltage and electromagnetic torque under fault condition can be revised as

$$\underline{V}_{qds} = r_s \underline{i}_{qds} + p \underline{\lambda}_{qds}, \quad (11)$$

$$\underline{Q}_r = \underline{v}_{brb_{qdr}} + r_r \underline{i}_{qdr} + p \underline{\lambda}_{qdr} - j \omega_r \underline{\lambda}_{qdr}, \quad (12)$$

$$T_e = -\left(\frac{27\sqrt{3}n}{16}\right)L_m \text{Im}\{\underline{i}_{qds}^* \underline{i}_{qdr}\}. \quad (13)$$

Eqs. (11)-(13) summarize the complex vector model of induction machine with broken rotor bars. With the model, it is convenient to simulate stator current under a number of broken rotor bars or even at different levels of severity by increasing the corresponding resistance value of R_b .

III. GRAPH-BASED FAULT SIGNATURE DETECTION

A. Fault Signature in Complex Space Vector Representation

For a healthy induction machine, its stator current contains a fundamental frequency component and harmonics of the fundamental frequency in inverter-fed applications. When a rotor bar is broken, an additional dominant frequency of $(1-2)sf$ is produced in the stator current. Therefore, the three-phase stator current for a faulty induction machine can be expressed as

$$i_a(t) = I_1 \cos(\omega_s t) + I_{brb} \cos(\omega_{brb} t + \phi_{brb}), \quad (14)$$

$$i_b(t) = I_1 \cos(\omega_s t - 2\pi/3) + I_{brb} \cos(\omega_{brb} t + \phi_{brb} - 2\pi/3), \quad (15)$$

$$i_c(t) = I_1 \cos(\omega_s t + 2\pi/3) + I_{brb} \cos(\omega_{brb} t + \phi_{brb} + 2\pi/3), \quad (16)$$

where I_1 and I_{brb} represents the amplitude of the fundamental component and the fault component, respectively; ω_s and $\omega_{brb} = (1-2s)\omega_s$ is the angular frequency of the power supply and of the fault component, respectively; and ϕ_{brb} is the phase angle of the fault component. In inverter-fed drive applications where the motor operation speed is variable, both ω_s and ω_{brb} are changing along with time.

According to complex space vector definition in (1), the stator current in complex space vector representation is

$$\begin{aligned} \underline{i}_s &= \frac{2}{3} (i_a(t) + \underline{a} i_b(t) + \underline{a}^2 i_c(t)) \\ &= I_1 e^{j\omega_s t} + I_{brb} e^{j(1-2s)\omega_s t}. \end{aligned} \quad (17)$$

The complex space vector defined in (17) can be referenced to a synchronous reference frame by applying the vector transformation

$$\underline{i}_{ss} = \underline{i}_s e^{-j\omega_s t} = I_1 + I_{brb} e^{-j(2s\omega_s)t}. \quad (18)$$

Note that the fundamental component I_1 is DC quantity. Since the DC component can be easily removed, the fault-related component at frequency of $2s\omega_s$ comes into play. We therefore define $I_{brb} e^{-j(2s\omega_s)t}$ as the signature of broken bar fault. It is clear that under variable speed operations, this fault signature is no longer a constant-frequency component, but a varying-frequency one. Therefore, due to the spreading out spectrum energy of the fault frequency, it is challenging for traditional MCSA methods to extract the fault signature as a single frequency component. In order to extract this fault signature of time-varying frequency, we propose to model the fault signature as a graph signal, with details introduced in the following subsection.

B. Graph Model of Fault Signature

A commonly used approach to processing a non-stationary signal is to represent it in the time-frequency domain using the short-time Fourier transform (STFT). The non-stationary signal is partitioned into short-time pieces using overlapped sliding-time windows. Each windowed piece of signal is analyzed using the FFT, providing frequency spectrum information within the local time duration.

By performing STFT on the transformed stator current \underline{i}_{ss} , a matrix of signal spectrogram $\mathbf{Y} = [\mathbf{Y}_1, \dots, \mathbf{Y}_m, \dots, \mathbf{Y}_M]$ is obtained, in which column vector \mathbf{Y}_m represents the frequency spectrum of the m^{th} windowed signal of the transformed stator current \underline{i}_{ss} . Each row of \mathbf{Y} corresponds to a fixed frequency value. To avoid redundancy, we only consider frequency range $[0, F_s/2]$, where F_s is the frequency sampling rate of stator current measurements. Since the operating speed and load is changing, the fault signature frequency is not a constant, meaning that the fault signature component in the spectrogram matrix does not lie in any single row vector of a certain frequency. Motivated by recent progress in graph signal processing, we treat the spectrogram of transformed stator current as a graph signal observed from graph $G = (\mathbf{V}, \mathbf{A})$, where $\mathbf{V} = \{v_1, \dots, v_m, \dots, v_M\}$ is the set of nodes, represented by sequential moving time windows, and $\mathbf{A} \in R^{M \times M}$ is the

graph shift, or a weighted adjacency matrix that represents the pairwise proximity between nodes, frequency spectrum $\mathbf{Y}_i \in C^k$ is then associated with the i^{th} node of the graph. We can estimate the graph shift \mathbf{A} through the STFT frequency spectra as

$$A_{i,j} = \frac{|\mathbf{Y}_i^H \mathbf{Y}_j|}{\sqrt{\mathbf{Y}_i^H \mathbf{Y}_i} \sqrt{\mathbf{Y}_j^H \mathbf{Y}_j}}, \text{ for } |i - j| < d, \quad (19)$$

where the superscript H indicates the matrix Hermitian transpose, d is the maximal distance of connected neighborhood nodes in the graph. Therefore, the spectrogram matrix of the stator current at varying speed and varying load can then be treated as a noisy graph signal with an unknown frequency shift due to the varying operation, *i.e.*,

$$\mathbf{Y}_m = \mathbf{X}_m \otimes \delta(\omega_m) + \mathbf{W}, \text{ for } m = 1, \dots, M, \quad (20)$$

where \otimes stands for convolutional operation; δ is the Dirac delta function; and \mathbf{W} is signal noise. $\mathbf{X} = [\mathbf{X}_1, \dots, \mathbf{X}_m, \dots, \mathbf{X}_M]$ represents the denoised spectrogram of constant frequency and constant load operation.

C. Graph-based Fault Signature Extraction

Inspired by recent research work on graph-model based signal denoising [14], [15], we extract the fault signature by solving an optimization problem as

$$\min_{\mathbf{x}, \{\omega_m\}} \sum_{m=1}^M \frac{1}{2} \|\mathbf{X}_m \otimes \delta(\omega_m) - \mathbf{Y}_m\|_2^2 + \lambda R_1(\mathbf{X}) + \beta R_2(\mathbf{X}), \quad (21)$$

where λ and β are hyper-parameters, $R_1(\mathbf{X})$ and $R_2(\mathbf{X})$ are regularizing terms. $R_1(\mathbf{X})$ imposes sparsity of the graph signal using L_1 norm as

$$R_1(\mathbf{X}) = |\mathbf{X}|_1 = \sum_{m=1}^M |\mathbf{X}_m|. \quad (22)$$

$R_2(\mathbf{X})$ promotes smoothness of graph signals, *i.e.*, neighboring nodes should share a similar fault signature in the frequency domain. $R_2(\mathbf{X})$ can be expressed as

$$R_2(\mathbf{X}) = \frac{1}{2} \|\mathbf{X} - \bar{\mathbf{A}}\mathbf{X}\|_F^2, \quad (23)$$

where $\bar{\mathbf{A}}$ is a normalized graph shift matrix whose entries are computed as $\bar{A}_{i,j} = \frac{A_{i,j}}{\sum_j A_{i,j}}$ to ensure that the sum of each row of $\bar{\mathbf{A}}$ equals to 1.

The goal is to recover \mathbf{X} and ω_m from \mathbf{Y} . The intuition behind the proposed graph-based denoising approach can be explained in two aspects: 1) the fault signature in each time window is a sparse (non-zero) component in the frequency spectrum and 2) the rotor fault frequency components in consecutive time windows are smoothly changing and have strong pairwise correlation. Once we obtain continuously changing sparse frequency components forming a curve in the spectrogram, we declare that we extract the fault signature.

The whole fault signature extraction problem can be summarized as the following stages.

- 1) Record the stator currents i_a, i_b, i_c and transform them into the complex vector \dot{i}_{ss} .
- 2) Apply STFT on \dot{i}_{ss} and remove the DC component to get the spectrogram matrix \mathbf{Y}
- 3) Solve optimization problem (21) [15]:
 - Estimate $\bar{\mathbf{A}}$;
 - Iteratively update ω_m and \mathbf{X} until convergence:

$$\omega_m = \operatorname{argmax}_{\omega} \frac{1}{2} \|\mathbf{X}_m \otimes \delta(\omega) - \mathbf{Y}_m\|_2^2, \quad (24)$$

$$\hat{\mathbf{X}} = (\mathbf{I} + \beta(\mathbf{I} - \bar{\mathbf{A}})^T(\mathbf{I} - \bar{\mathbf{A}}))^{-1}([\mathbf{Y}_m \otimes \delta(-\omega_m)]), \quad (25)$$

$$\mathbf{X} = \operatorname{sign}(\hat{\mathbf{X}}) \max(|\hat{\mathbf{X}}| - \lambda, 0), \quad (26)$$

where \mathbf{I} is an identity matrix.

- 4) Output fault signature $\hat{\mathbf{Y}}_m = \mathbf{X}_m \otimes \delta(\omega_m)$.

IV. SIMULATION

A MATLAB/Simulink model of inverter-fed induction machine with broken rotor bar is shown in Fig. 2, where each block function represents one or more corresponding model equations shown in Section II. A simple Volt-per-Hertz (V/f) control scheme is used to control the induction motor [16]–[18]. The stator current in the complex space vector representation is stored to the workplace for further analysis. The complex vector model of induction machine with broken rotor bar in Section II is successfully realized in three simulations.

First, we check the operation of a healthy machine with a constant load. The motor speed is accelerated by increasing the supply frequency from 0 Hz to 60 Hz. When the motor is operating in a healthy condition, the STFT power spectrum of the stator current \dot{i}_{ss} is shown in Fig. 3 (a), where we only observe a dominant DC component in the transformed space. Fig. 3 (b) shows the denoised signal using our graph-based method on Fig. 3 (a), where no continuous changing but two isolated frequency segments are observed. Fig. 3 (c) depicts the theoretical frequency component of operation.

Second, we examine the operation of a faulty machine at a varying speed with a constant load, where two rotor bars are broken in the model. The corresponding STFT power spectrum of the stator current \dot{i}_{ss} is shown in Fig. 4 (a) for comparison, where we can observe a time-varying fault signature frequency component. Fig. 4 (b) shows the extracted fault signature using our proposed graph-based method, which agrees with the theoretical result as depicted in Fig. 4 (c).

Third, we examine the operation of the same faulty machine at a varying speed with a varying load. The machine is starting from 0 Hz and accelerating to 60 Hz with an extra load applied at 8s. The corresponding simulation result is shown in Fig. 5. Similar to Fig. 4, we can extract the fault signature using our proposed graph-based method, which is also well matched with the theoretical one as depicted and Fig. 5 (c).

From all above simulations, it is clear that the proposed graph-based method is capable of detecting rotor fault under varying speeds and varying load conditions.

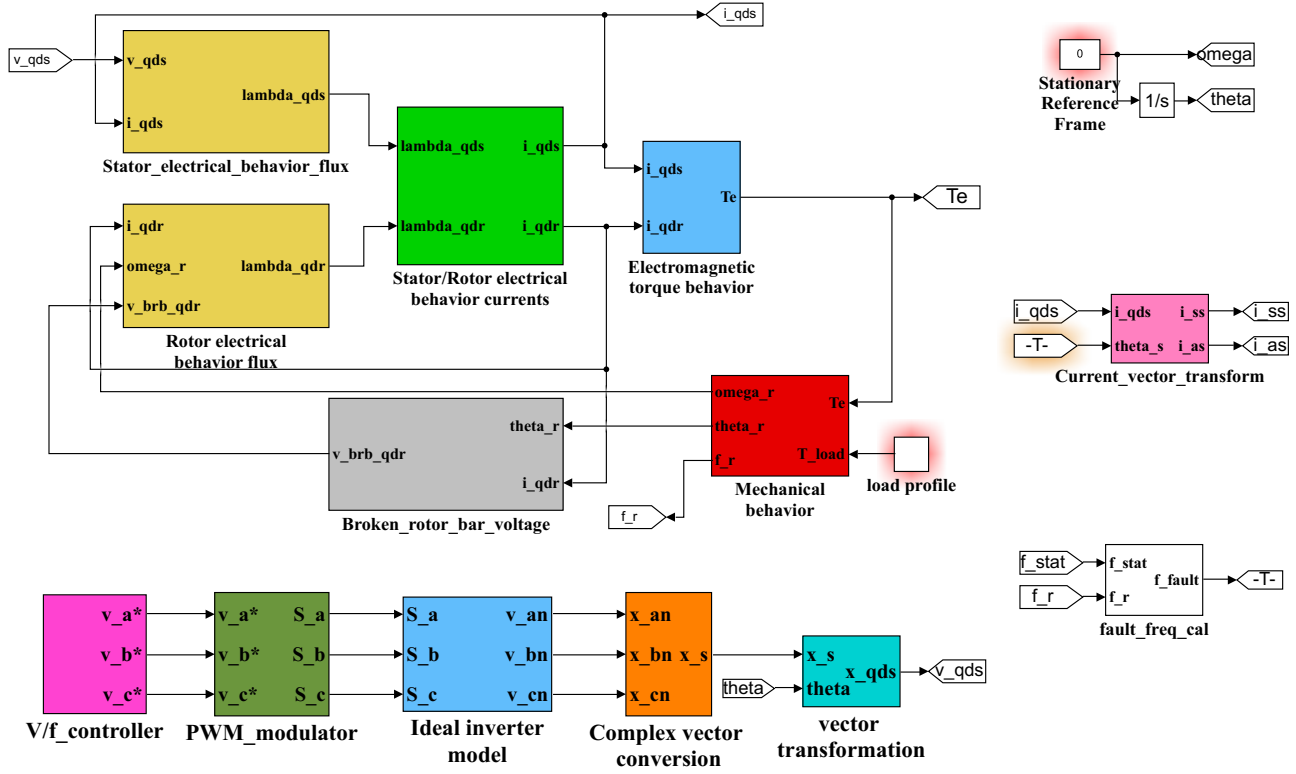


Fig. 2. Simulation model of inverter-fed induction machine with/without broken-rotor-bar fault.

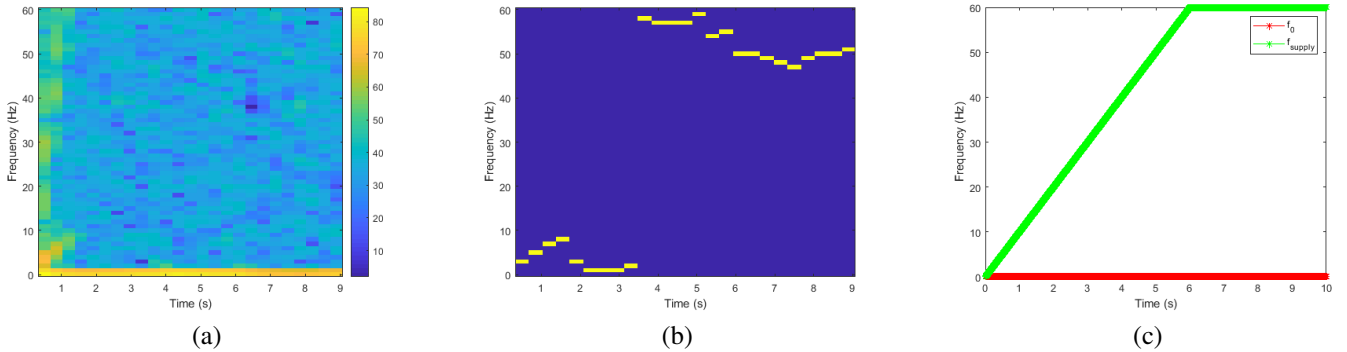


Fig. 3. Simulation results of healthy induction motor at varying speed and constant load (a) STFT spectrum, (b) denoised signal without continuously changing fault signature, and (c) theoretical operational frequency component trajectory in the original space (green) and the complex vector space (red).

V. CONCLUSION

We studied broken-rotor-bar fault detection for the inverter-fed squirrel-cage induction motor under varying speed and varying load conditions, and defined a fault signature using complex space vector notation. To extract the fault signature, we proposed a graph-based method by solving an optimization problem with constraints imposing smoothness and sparsity of the fault signature. Simulation results demonstrate that our proposed method can effectively extract fault signature under varying speed and varying load operations. The newly revealed fault signature detection method is applicable for both line-fed and inverter-fed induction motor drives.

REFERENCES

- [1] Anibal T De Almeida, Fernando JTE Ferreira, and Ge Baoming, "Beyond induction motors – technology trends to move up efficiency," *IEEE Transactions on Industry Applications*, vol. 50, no. 3, pp. 2103–2114, 2013.
- [2] Fiorenzo Filippetti, Alberto Bellini, and Gerard-Andre Capolino, "Condition monitoring and diagnosis of rotor faults in induction machines: State of art and future perspectives," in *2013 IEEE Workshop on Electrical Machines Design, Control and Diagnosis (WEMDCD)*. IEEE, 2013, pp. 196–209.
- [3] Fiorenzo Filippetti, Giovanni Franceschini, Carla Tassoni, and Peter Vas, "AI techniques in induction machines diagnosis including the speed ripple effect," *IEEE Transactions on Industry Applications*, vol. 34, no. 1, pp. 98–108, 1998.
- [4] Angel Sapena-Bano, Jordi Burriel-Valencia, Manuel Pineda-Sanchez, Ruben Puche-Panadero, and Martin Riera-Guasp, "The harmonic order

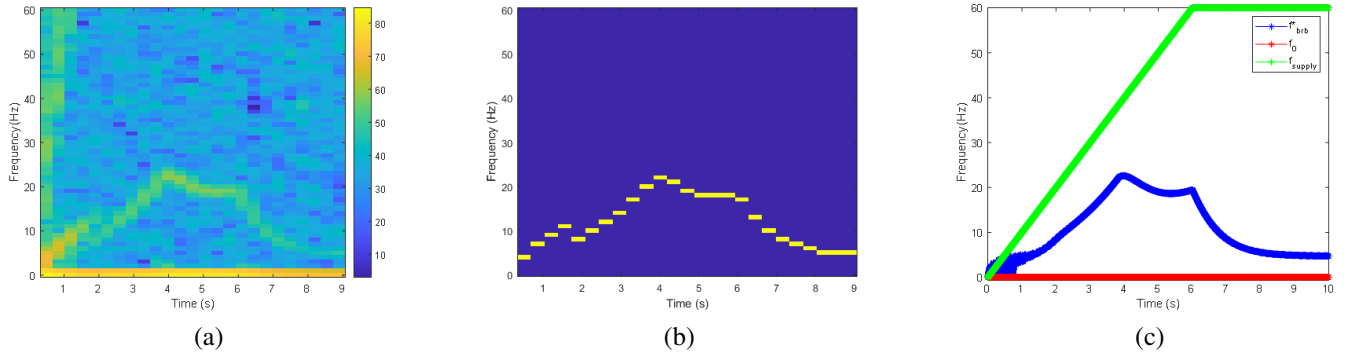


Fig. 4. Simulation results of faulty induction motor with a varying speed and a constant load: (a) STFT spectrum, (b) Extracted fault signature using graph-based method, and (c) theoretical fault signature (blue) and operational frequency in the original space (green) and the complex vector space (red).

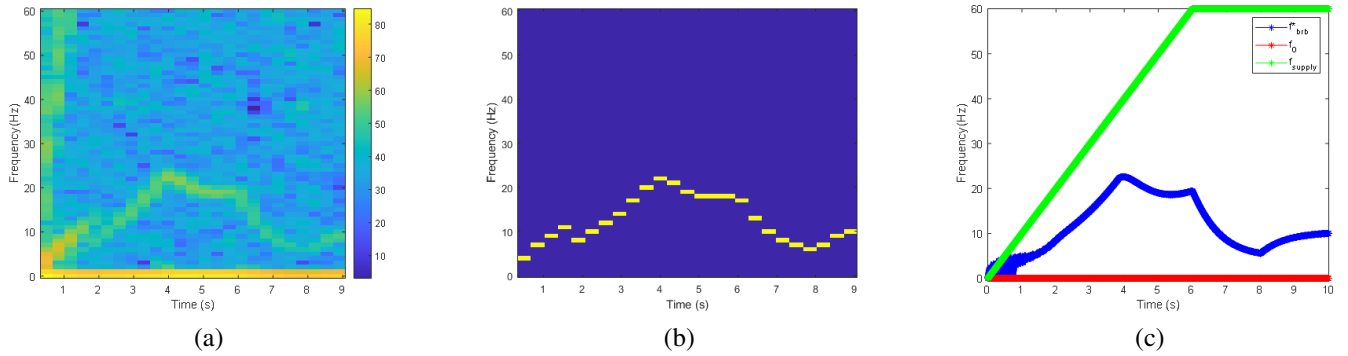


Fig. 5. Simulation results of faulty induction motor with a varying speed and a varying load: (a) STFT spectrum, (b) Extracted fault signature using graph-based method, and (c) theoretical fault signature (blue) and operational frequency in the original space (green) and the complex vector space (red).

tracking analysis method for the fault diagnosis in induction motors under time-varying conditions,” *IEEE Transactions on Energy Conversion*, vol. 32, no. 1, pp. 244–256, 2016.

- [5] Jordi Cusidó Cusido, Luis Romeral, Juan A Ortega, Javier A Rosero, and Antonio García García Espinosa, “Fault detection in induction machines using power spectral density in wavelet decomposition,” *IEEE Transactions on Industrial Electronics*, vol. 55, no. 2, pp. 633–643, 2008.
- [6] Vanessa Fernandez-Cavero, Daniel Morinigo-Sotelo, Oscar Duque-Perez, and Joan Pons-Llinares, “A comparison of techniques for fault detection in inverter-fed induction motors in transient regime,” *IEEE Access*, vol. 5, pp. 8048–8063, 2017.
- [7] Tomas Alberto Garcia-Calva, Daniel Morinigo-Sotelo, and Rene de Jesus Romero-Troncoso, “Non-uniform time resampling for diagnosing broken rotor bars in inverter-fed induction motors,” *IEEE Transactions on Industrial Electronics*, vol. 64, no. 3, pp. 2306–2315, 2016.
- [8] Tomas Alberto Garcia-Calva, Daniel Morinigo-Sotelo, Arturo Garcia-Perez, David Camarena-Martinez, and Rene de Jesus Romero-Troncoso, “Demodulation technique for broken rotor bar detection in inverter-fed induction motor under non-stationary conditions,” *IEEE Transactions on Energy Conversion*, vol. 34, no. 3, pp. 1496–1503, 2019.
- [9] Dehong Liu and Dingguo Lu, “Off-the-grid compressive sensing for broken-rotor-bar fault detection in squirrel-cage induction motors,” *IFAC-PapersOnLine*, vol. 48, no. 21, pp. 1451–1456, 2015.
- [10] Jongwan Kim, Sungsik Shin, Sang Bin Lee, Konstantinos N Gyftakis, M’hamed Drif, and Antonio J Marques Cardoso, “Power spectrum-based detection of induction motor rotor faults for immunity to false alarms,” *IEEE Transactions on Energy Conversion*, vol. 30, no. 3, pp. 1123–1132, 2015.
- [11] M’hamed Drif and Antonio J Marques Cardoso, “Stator fault diagnostics in squirrel cage three-phase induction motor drives using the instantaneous active and reactive power signature analyses,” *IEEE Transactions on Industrial Informatics*, vol. 10, no. 2, pp. 1348–1360, 2014.
- [12] Xiaogang Luo, Yuefeng Liao, Hamid A Toliyat, Ahmed El-Antably, and Thomas A Lipo, “Multiple coupled circuit modeling of induction machines,” *IEEE Transactions on industry applications*, vol. 31, no. 2, pp. 311–318, 1995.
- [13] Alfredo R Munoz and Thomas A Lipo, “Complex vector model of the squirrel-cage induction machine including instantaneous rotor bar currents,” *IEEE transactions on industry applications*, vol. 35, no. 6, pp. 1332–1340, 1999.
- [14] Siheng Chen, Aliaksei Sandryhaila, José MF Moura, and Jelena Kovacevic, “Signal denoising on graphs via graph filtering,” in *2014 IEEE Global Conference on Signal and Information Processing (GlobalSIP)*. IEEE, 2014, pp. 872–876.
- [15] Dehong Liu, Siheng Chen, and Petros T Boufounos, “Graph-based array signal denoising for perturbed synthetic aperture radar,” in *IGARSS 2020-2020 IEEE International Geoscience and Remote Sensing Symposium*. IEEE, 2020, pp. 1881–1884.
- [16] Zhe Zhang, Yiqi Liu, and Ali M Bazzi, “An improved high-performance open-loop v/f control method for induction machines,” in *2017 IEEE Applied Power Electronics Conference and Exposition (APEC)*. IEEE, 2017, pp. 615–619.
- [17] Zhe Zhang and Ali M Bazzi, “Robust sensorless scalar control of induction motor drives with torque capability enhancement at low speeds,” in *2019 IEEE International Electric Machines & Drives Conference (IEMDC)*. IEEE, 2019, pp. 1706–1710.
- [18] Zhe Zhang, Muhammed Ali Gultekin, and Ali M Bazzi, “State-space modeling of multi-mode-controlled induction motor drive,” in *2021 IEEE International Electric Machines & Drives Conference (IEMDC)*. IEEE, 2021, pp. 1–5.